IS-T-812

DECAY OF MASS-SEPARATED ^{118}Ag TO LEVELS IN ^{118}Cd

Deborah Reed Margetan

M. S. Thesis Submitted to Iowa State University

Ames Laboratory DOE
Iowa State University
Ames, Iowa 50011

Date Transmitted: April 1978

PREPARED FOR THE U.S. DEPARTMENT OF ENERGY
UNDER CONTRACT NO. W-7405-eng-82

DISCLAIMER

NOTICE

Printed in USA

Available from: National Technical Information Service
U. S. Department of Commerce
P.O. Box 1553
Springfield, VA 22161

Price: Microfiche $3.00
Paper Copy $4.50

IS-T-812

Decay of mass-separated ^{118}Ag to levels in ^{118}Cd

Deborah Reed Margetan

Under the supervision of John C. Hill
From the Department of Physics
Iowa State University

A study of the gamma-ray de-excitation following the beta decay of ^{118}Ag using the TRISTAN on-line isotope separator is reported. Gamma-ray singles, gamma-gamma coincidence, and gamma-ray multiscale measurements were made using Ge(Li) detectors. A total of 52 gamma rays were observed in the decay of ^{118}Ag. Thirty-eight of these were placed in a level scheme for ^{118}Cd consisting of 20 excited states up to 3382 keV. Gamma-ray multiscale measurements indicated that ^{118}Ag has an isomeric state at 128 keV with a half-life of 2.0 ± 0.2 seconds. The ground state half-life is 3.76 ± 0.15 seconds. The ^{118}Ag decay scheme is compared with a previcus decay study. The level scheme systematics are discussed and compared with recent collective model calculations.

Decay of mass-separated ^{118}Ag to levels in ^{118}Cd

by

Deborah Reed Margetan

A Thesis Submitted to the
Graduate Faculty in Partial Fulfillment of
The Requirements for the Degree of
MASTER OF SCIENCE

Department: Physics
Major: Nuclear Physics

Approved:

_____
In Charge of Major Work

_____
For the Major Department

_____
For the Graduate College

Iowa State University
Ames, Iowa

1978

TABLE OF CONTENTS

LIST OF FIGURES

LIST OF TABLES

I. INTRODUCTION

A. Basis for the Study of ^{118}Ag

Unstable neutron-rich nuclei tend to decay via processes which cause the ratio of protons to neutrons to increase. The nucleus ^{118}Ag undergoes beta decay, in which a neutron changes into a proton while an electron and an antineutrino are simultaneously created and emitted. The resulting daughter nucleus is frequently in an excited state. It then de-excites to its ground state by emitting gamma rays or conversion electrons. The energies and intensities of these gamma rays can be measured, and this information can be used to determine the energies of states in the ^{118}Cd daughter. Figure 1 shows the beta-decay chain for A=118.

Nuclear spectroscopic data is studied for systematics that will yield new insight into nuclear structure. Certain values of Z(proton number) and N(neutron number) called "magic numbers" are associated with exceptionally interesting nuclei. Magic isotopes and isotones have unusually large binding energies per nucleon and other properties which make them important in nuclear theory, much as the noble gases were important to the development of atomic physics. The nucleus ^{118}Cd(Z=48) is theoretically interesting since it is only two proton numbers away from the magic number Z=50.

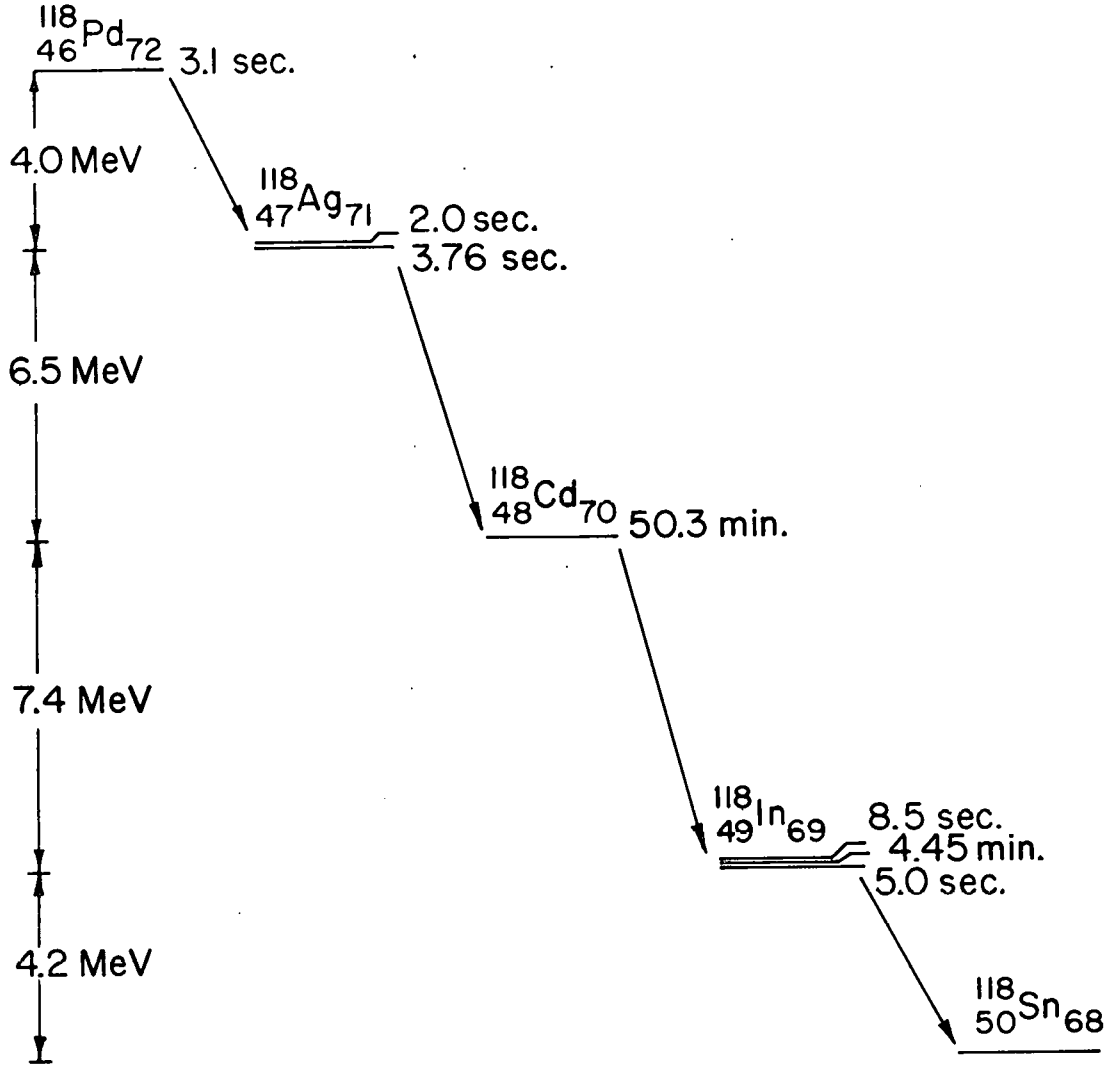

Figure 1. A=118 beta-decay chain studied in this work

A theoretical model is sometimes based on spectroscopic information from a specific nucleus. If the model is successful, it can then be applied to other nuclei which possess similar structures. The particular model discussed in this work is a rotation-vibration collective model. It is an extension of the model developed by Davydov and Chaban, which is discussed in Ref. 1 and 2. It assumes that the nucleus is permanently deformed and undergoes both rotations and breathing-mode vibrations. The model has been successfully applied to even-even Pd(Z=46) isotopes by H. H. Hsu, S. A. Williams, F. K. Wohn, and F. J. Margetan (3). The TRISTAN group has undertaken a study of several even-even Cd isotopes in order to see if the model can be applied with equal success to Z=48 nuclei. In Chapter V, details of the model are briefly discussed and a comparison is made for ^{118}Cd between results from this experiment and the above theory.

B. Survey of Earlier Work

The first observation of ^{118}Ag decay was reported by K. Fritze and K. Griffiths in 1967 (4). The Ag activity was obtained by chemical separation from ^{235}U fission-products. The ^{118}Ag half-life was determined to be approximately 5 seconds.

In 1968 H. V. Weiss, J. M. Fresco, and W. L. Reichert reported a half-life of 5.3 ± 0.9 seconds (5). In their experiment, they chemically separated ^{118}Ag from thermal neutron-irradiated ^{235}U after fission. In 1969 H. V. Weiss, N. E. Ballou, J. L. Elzie, and J. M. Fresco published the results of another chemical-separation study (6). A half-life of 5.6 ± 0.2 seconds was measured.

In 1971 B. Fogelberg, A. Bäcklin, and T. Nagarajan reported the energy levels of ^{118}Cd populated in the beta decay of ^{118}Ag (7). The Ag activity was obtained at the OSIRIS on-line mass-separator facility at Studsvik (8). Gamma-ray singles, gamma-gamma coincidence, and multiscale measurements were made. For the first time, a long-lived excited state in ^{118}Ag was observed. This isomeric state was 128 keV above the ground state. Its half-life was measured to be 2.8 ± 0.3 seconds. The ground state half-life was determined to be 3.7 ± 0.2 seconds. On the order of 100 gamma rays were detected but energies were given for only eight of them. These eight were placed in a level scheme for ^{118}Cd consisting of seven excited levels. Tentative spin and parity assignments were made. The Studsvik group's results will be compared with those of this work in Chapter V.

II. EXPERIMENTAL METHODS

A. The TRISTAN System

This project is one of many studies of ^{235}U fission products being conducted at the TRISTAN facility at the Ames Laboratory Research Reactor. Except for TRISTAN's new method of producing fission products, the TRISTAN system has been thoroughly described in an article by J. R. McConnell and W. L. Talbert (9). Thus only a brief description of the system will be reported in this work.

The TRISTAN facility consists of an on-line isotope separator and a switch magnet which guides the ion beam to one of three stations. These stations are equipped with different types of nuclear spectroscopic equipment. The layout of the TRISTAN facility is shown in Figure 2.

In the past, the TRISTAN facility has only been capable of separating the gaseous fission products krypton and xenon. However, a new "in-beam" ion source based on the Studsvik design (8) has been developed for the system which allows the separation of many nongaseous fission products. The fission product activity is produced when the in-beam target-ion source combination is placed in an external neutron beam of 3×10^9 neutrons/cm^2-sec emanating from the reactor. The neutrons travel from the reactor to the ion source via a tapered beam tube and through a laminated steel

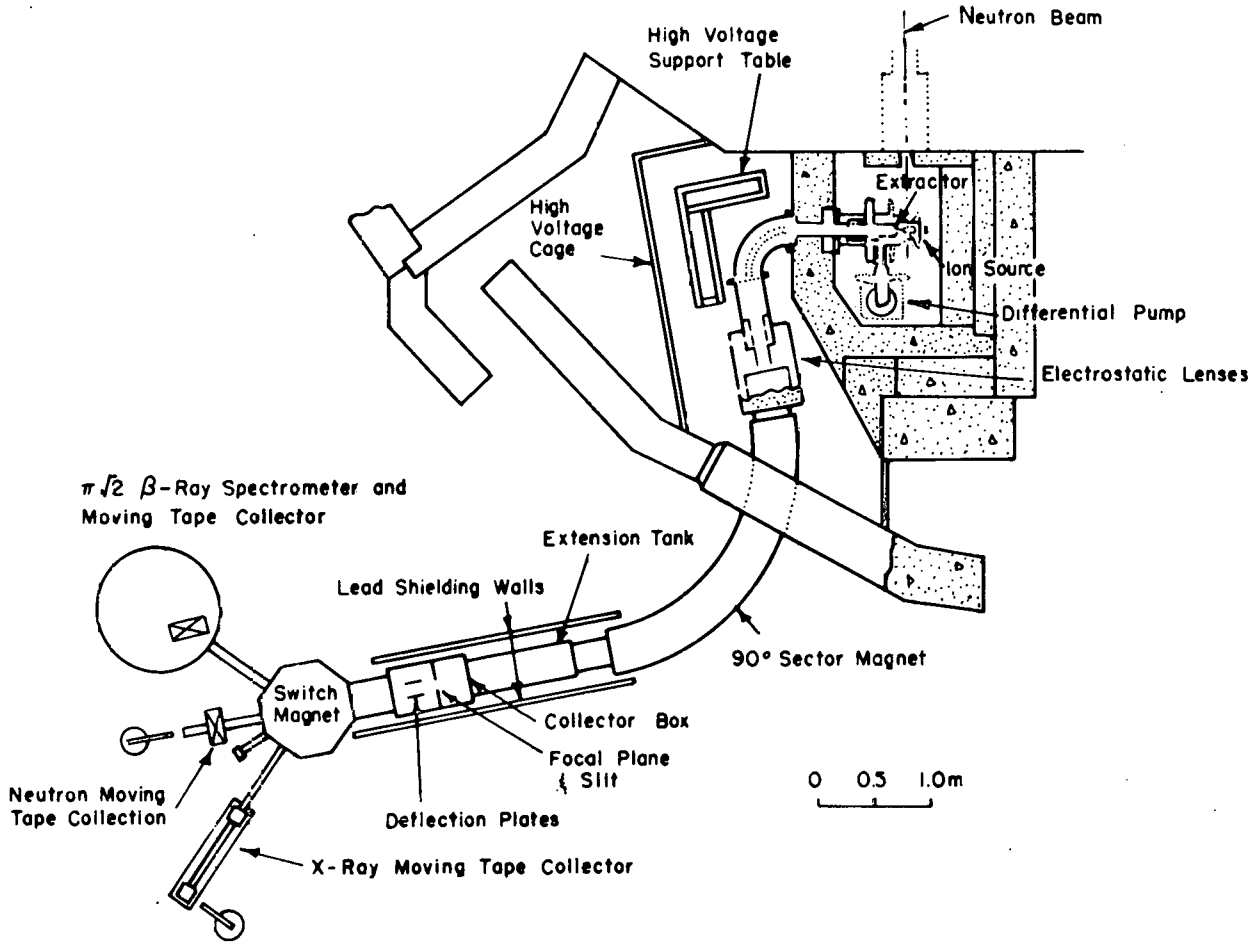

Figure 2. Schematic layout of the TRISTAN isotope-separator facility

and masonite rotary shutter. The beam can be shut off by rotating the shutter 90° and filling the beam tube with water. The target is a graphite cloth sleeve containing $^{235}UO_2$ which is fitted inside the cylindrical graphite anode. A diagram of the in-beam ion source is shown in Figure 3.

During separator operation, thermalized fission products diffuse into the plasma in the central region of the anode. A sweep gas which is a mixture of helium with a few percent stable krypton and xenon is used to help sustain a plasma discharge in the ion source. In addition, the krypton and xenon are useful as mass markers and aid in focusing and monitoring the mass number of the ion beam.

The ionized sweep gas and fission products are next accelerated through a 50-kilovolt potential and focused by two electrostatic lenses. Then the beam enters the 90° analyzing magnet which mass-separates the ionized fission products. After passing through this magnet, the mass-separated beam enters a collector box where the beam can be focused visually by observing the stable krypton and xenon lines on a fluorescent screen. The magnet current is then adjusted so that the desired mass passes through a slit in the collector box.

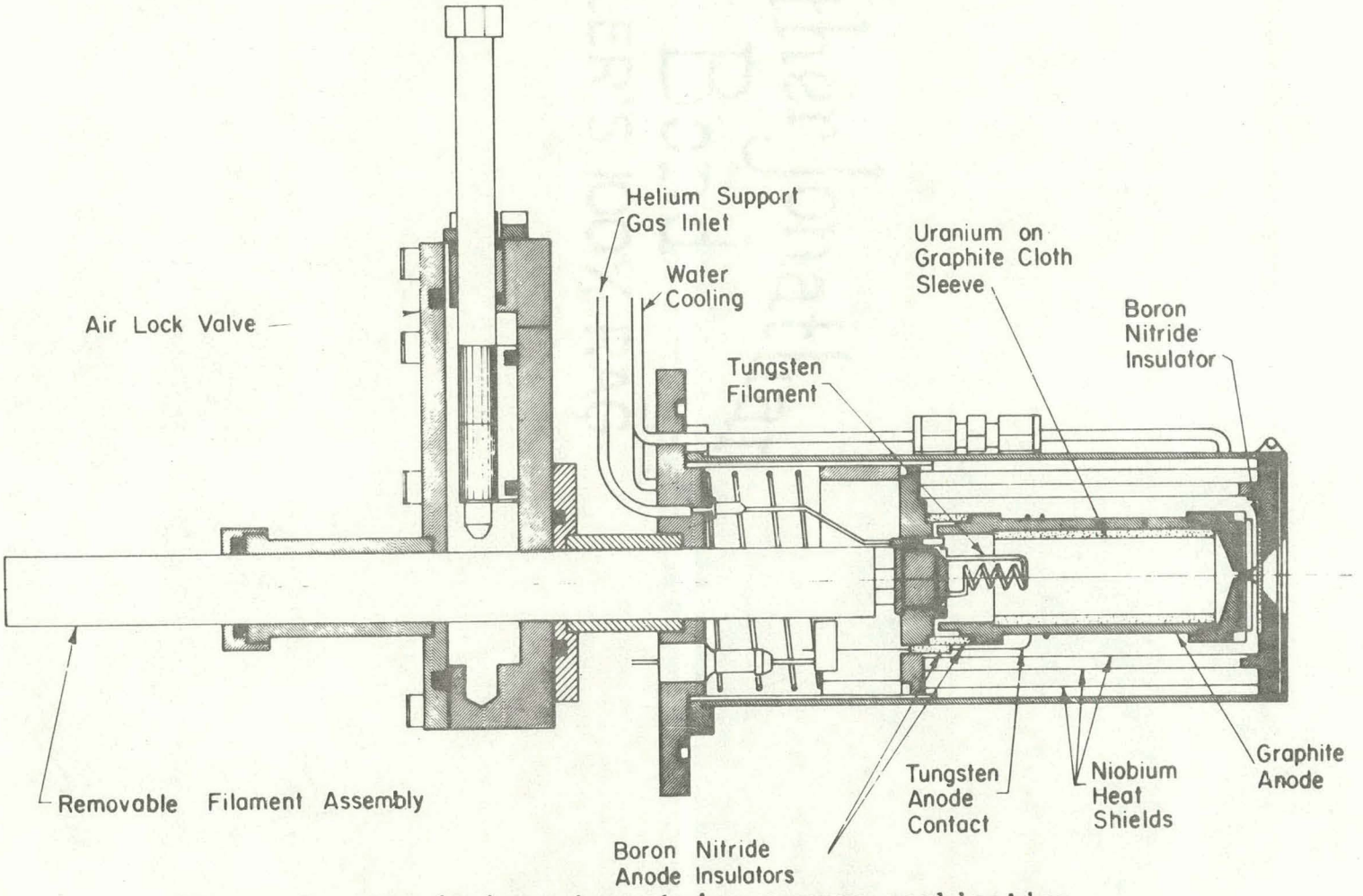

Figure 3. New in-beam target-ion source combination

The collector box slit is aligned with the switch magnet entrance. For this project, the magnet was set to guide the beam to the moving tape collector (MTC) which was controlled by the daughter analysis system (DAS). The switch magnet also provides a second stage of mass separation.

In this experiment, the beam deposited on the aluminum-coated mylar tape of the MTC consisted of the activities of ^{118}Ag and its daughters. The isobaric enhancement of the daughter activities is performed mechanically. By adjusting the beam collection, delay, and accumulation times for the tape motion, it is possible to independently enhance a desired activity. The MTC system has both "parent" and "daughter" port positions for the detectors. The minimum delay time is the time needed to transfer the activity from the parent port to the daughter port. While the tape is in motion, the beam is deflected by a voltage across the deflection plates and the multichannel analyzer is gated off. The DAS controls the cycling of the tape, the deflection voltage, and the analyzer. In the next section, an example of isobaric enhancement using the MTC is given.

B. Gamma-ray Measurements

1. Gamma-ray singles measurements

Singles data was obtained using LEPS(Low Energy Photon Spectrometer) and large Ge(Li) detectors. The large volume detectors had efficiencies of about 15%. A block diagram of the electronic circuit used to accumulate gamma-ray singles spectra is shown in Figure 4. During the 30-hour ^{118}Ag singles experiment, three spectra were collected at the parent port: an 8K spectrum with an energy range of 0-4 MeV, an 8K spectrum with an energy range of 2.5-8 MeV, and a 4K LEPS spectrum with an energy range of 0-400 keV. In order to reduce contamination from the daughter activities ^{118}Cd ($T_{\frac{1}{2}}$=50.3 min.), ^{118}In^{m} ($T_{\frac{1}{2}}$=4.45 min.), and ^{118}In ($T_{\frac{1}{2}}$=5.0 sec.),the MTC was set to accumulate activity for 6 seconds. At the end of this period the tape was moved. Calibration and mixed calibration runs were made so that standard gamma rays from ^{56}Co, ^{137}Cs, and ^{182}Ta could be used to obtain detector energy and intensity calibrations and to map the nonlinearities of the system. To facilitate identification of Ag gamma rays, a daughter spectrum was collected at the daughter port. In order to enhance the long-lived ^{118}Cd and ^{118}In, the MTC was set to accumulate activity for 120 seconds and then delay for 30 seconds before counting so that all of the ^{118}Ag activity had decayed. Background runs

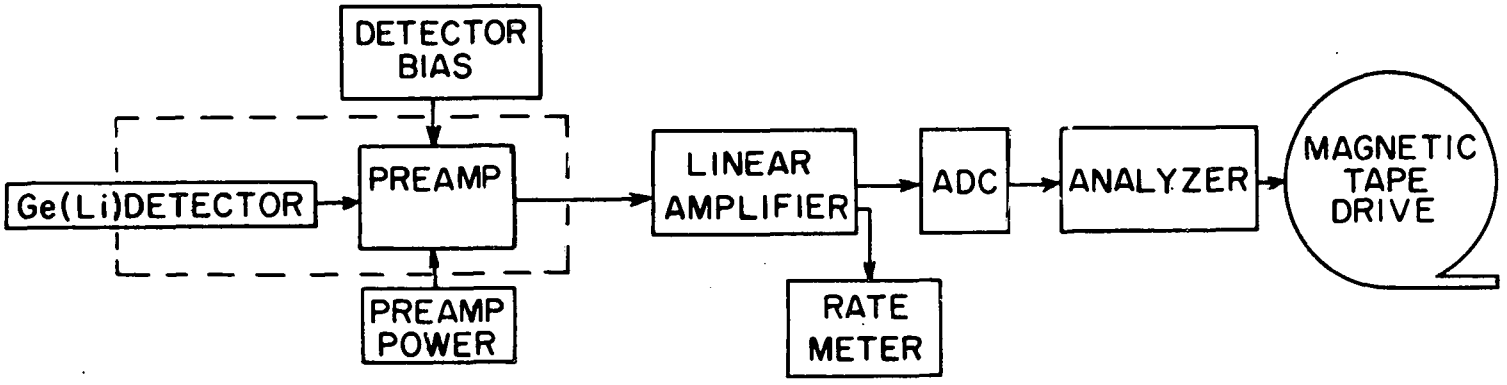

Figure 4. Block diagram of gamma singles electronics

were also made at both the parent and daughter ports so that background activity could be easily distinguished from Ag activity.

The ^{118}Ag nucleus beta decays from both the ground state and a short-lived isomeric state. In order to distinguish between gammas from the two decays, a one-hour singles experiment was conducted in which the short-lived decay was suppressed. The MTC was set to accumulate for 8.0 seconds and then delay for 6.0 seconds before counting. One 4K spectrum was collected at the parent port and another 4K spectrum was collected at the daughter port. The short-lived decay was suppressed in the daughter port spectrum.

2. Multiscale measurements

The half-lives of both ^{118}Ag isomers were remeasured in a multispectral scaling experiment. A diagram of the multiscale electronics is shown in Figure 5. In all measurements the gamma-ray spectra were multiscaled into 16 time bins which each contained 1024 channels of information. The energy range of each bin was 0-550 keV.

The ground state half-life of ^{118}Ag was determined from the decay of the 488-keV gamma ray. The MTC was set to collect for 6 seconds and delay for one second. The time width of each bin was one second. The length of this run was about 20 hours.

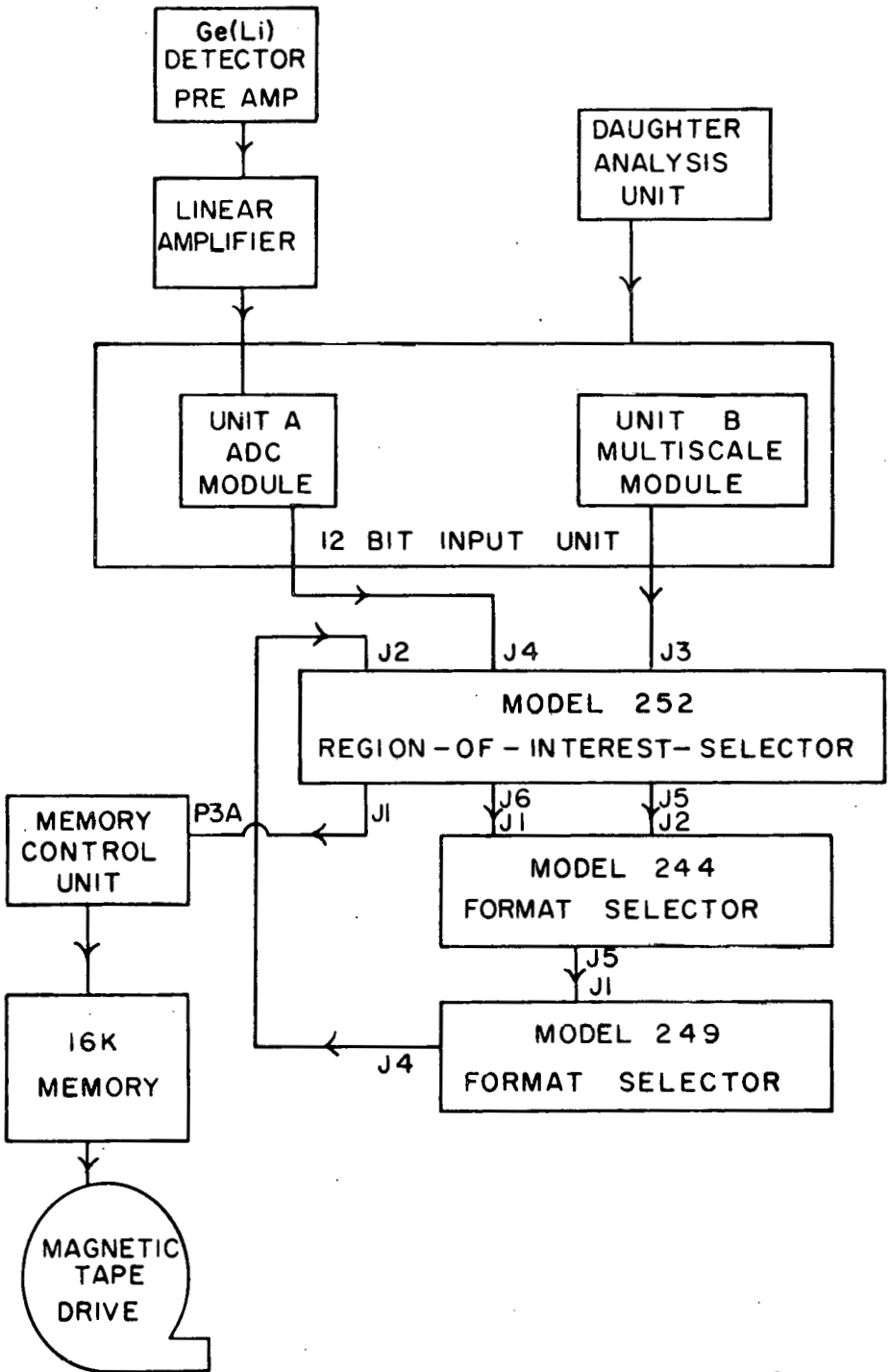

Figure 5. Block diagram of multiscale electronics

The isomeric half-life was obtained from the decay of the 128-keV gamma ray. The MTC was set to collect for 3 seconds and to delay for 6.4 seconds. The time width of each bin was .4 seconds. The length of this run was about 12 hours.

3. Gamma-gamma coincidence measurements

Two Ge(Li) detectors were positioned in 180° geometry for a 17-hour coincidence study. Each detector had two preamplifier outputs. One was used to detect coincidence events and the other was used for energy analysis. The MTC was set to collect for 30 seconds and delay for 6 seconds.

A block diagram of the coincidence electronics is shown in Figure 6. Constant-fraction timing was used because the resulting time signal could first be compensated for amplitude and rise time. This timing technique is described in two articles by D. A. Gedcke and W. J. McDonald (10,11).

The timing between signals from the two detectors determined a coincidence event. The logic signal from one detector was used as a start signal for the time-to-pulse-height converter (TPHC). The signal from the other detector was delayed for about 40 ns and acted as a stop signal for the TPHC. The single channel analyzer (SCA) then selected a region of TPHC pulse heights which corresponded to coincidence events. Whenever the TPHC output fell within this

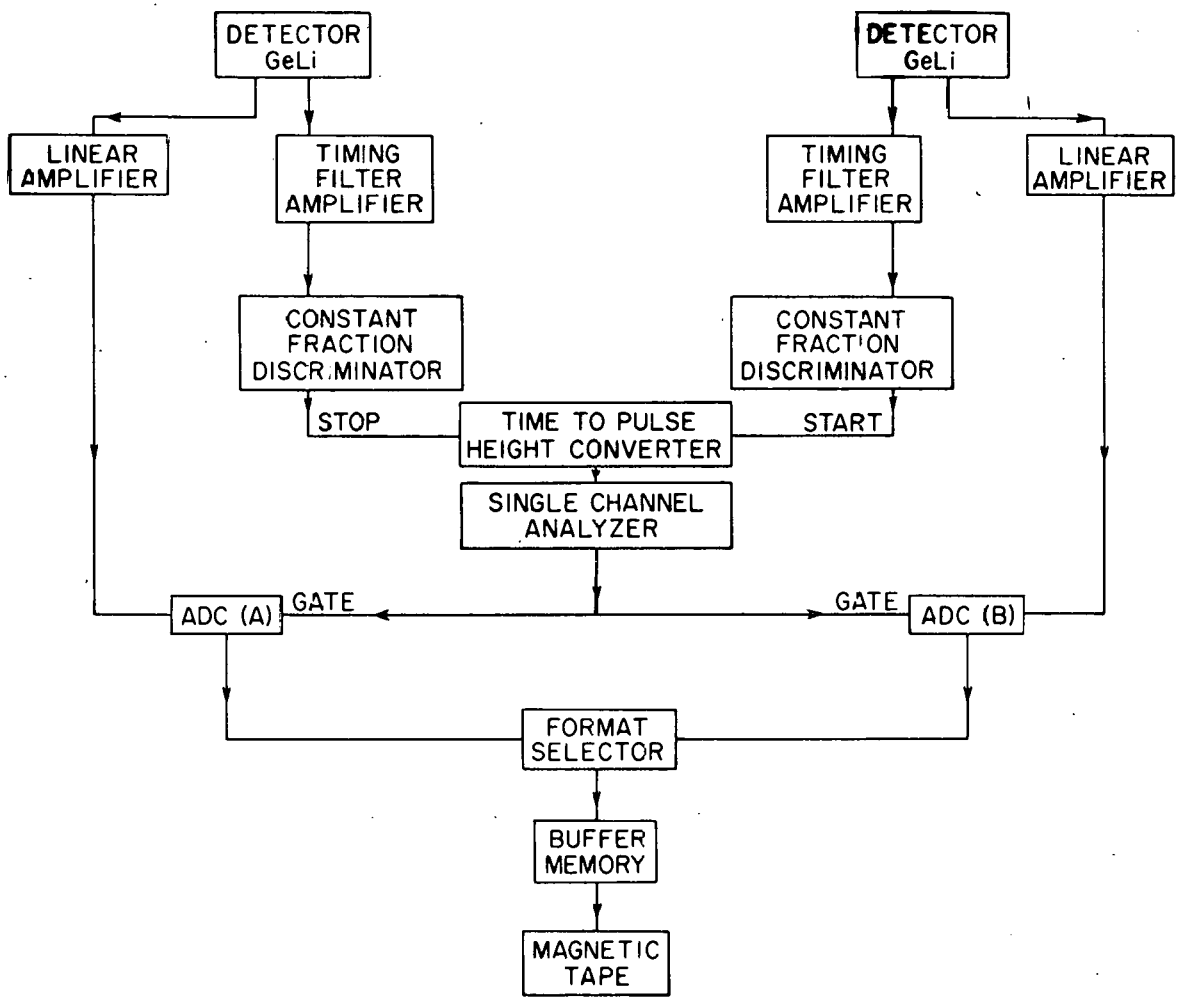

Figure 6. Block diagram of gamma coincidence electronics

coincidence window, the SCA sent an output signal to gate the two ADC's to accept the energy signals. The ADC's were set in the 4K mode so that each incoming pair of events was registered in a 4K channel x 4K channel coincidence array. The coincidence pairs were stored in a buffer system. After the buffer had recorded 2048 events, the data was dumped onto a magnetic tape and the process was repeated.

III. DATA ANALYSIS AND RESULTS

Over the years members of the TRISTAN group have developed computer programs to help in the analysis of the vast amounts of data generated by experiments performed at the TRISTAN facility. Several of the programs are briefly discussed in this chapter, and the results of the computer analysis performed on the ^{118}Ag decay data are given. Summaries of the results are shown in several figures and tables.

A. Transition Energies and Intensities

The multichannel analyzer (MCA) data were recorded periodically on magnetic tape in order to avoid memory overflows and gain-shift distortions. The computer program DISKRITE was used to add appropriate MCA spectra together and write the sum onto TRISTAN's private disk.

The computer program UNIPLOT was used to obtain plots of the data. These plots indicated that only the 0-4 Mev spectrum needed to be analyzed. No ^{118}Ag gammas, other than those in the above spectrum, appeared in the high-energy spectrum or in the low-energy LEPS spectrum. The LEPS spectrum is shown in Figure 7, and the Ag spectrum from the Ge(Li) detector appears in Figure 8.

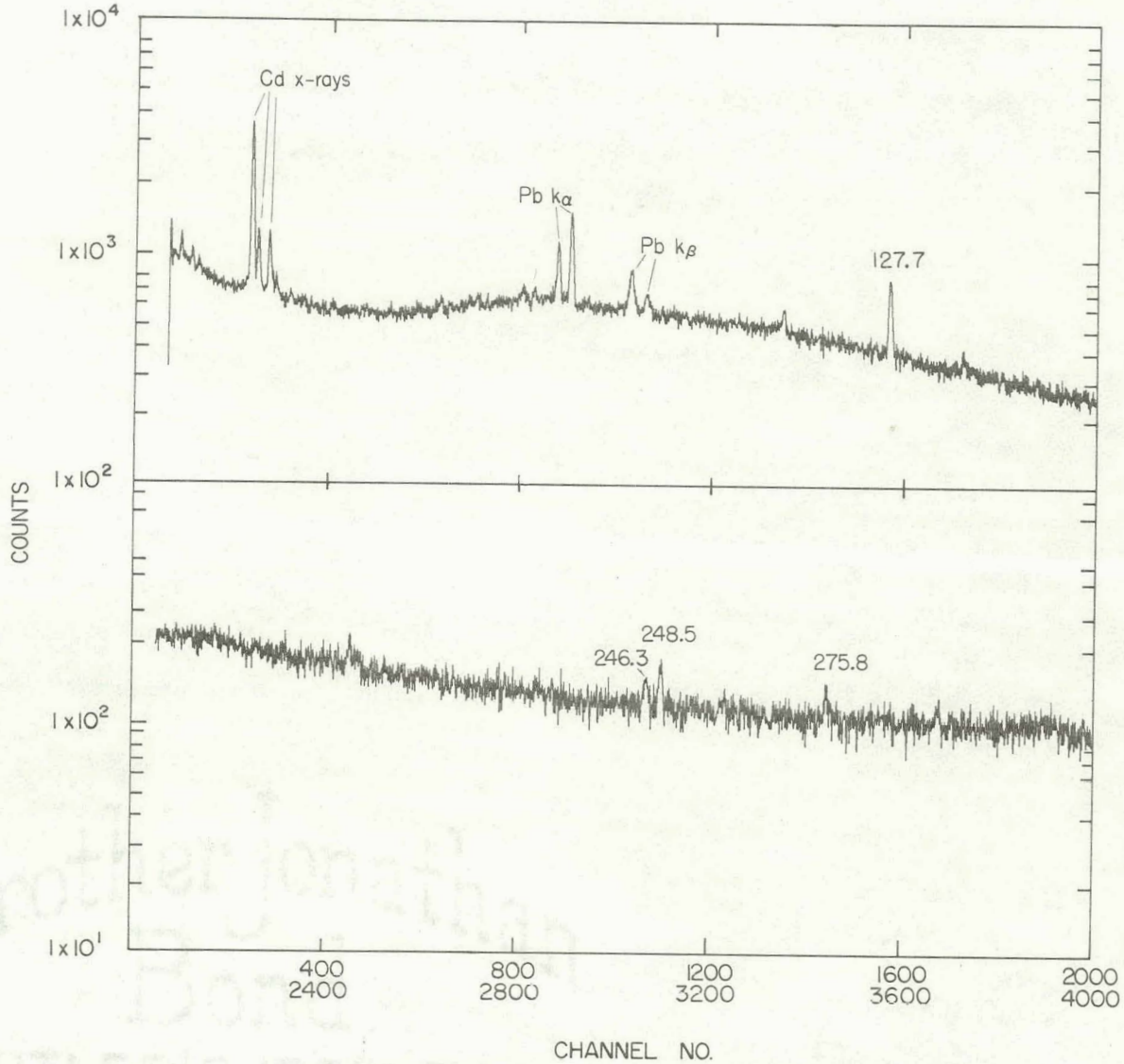

Figure 7. LEPS gamma-ray spectrum from the decay of ^{118}Ag

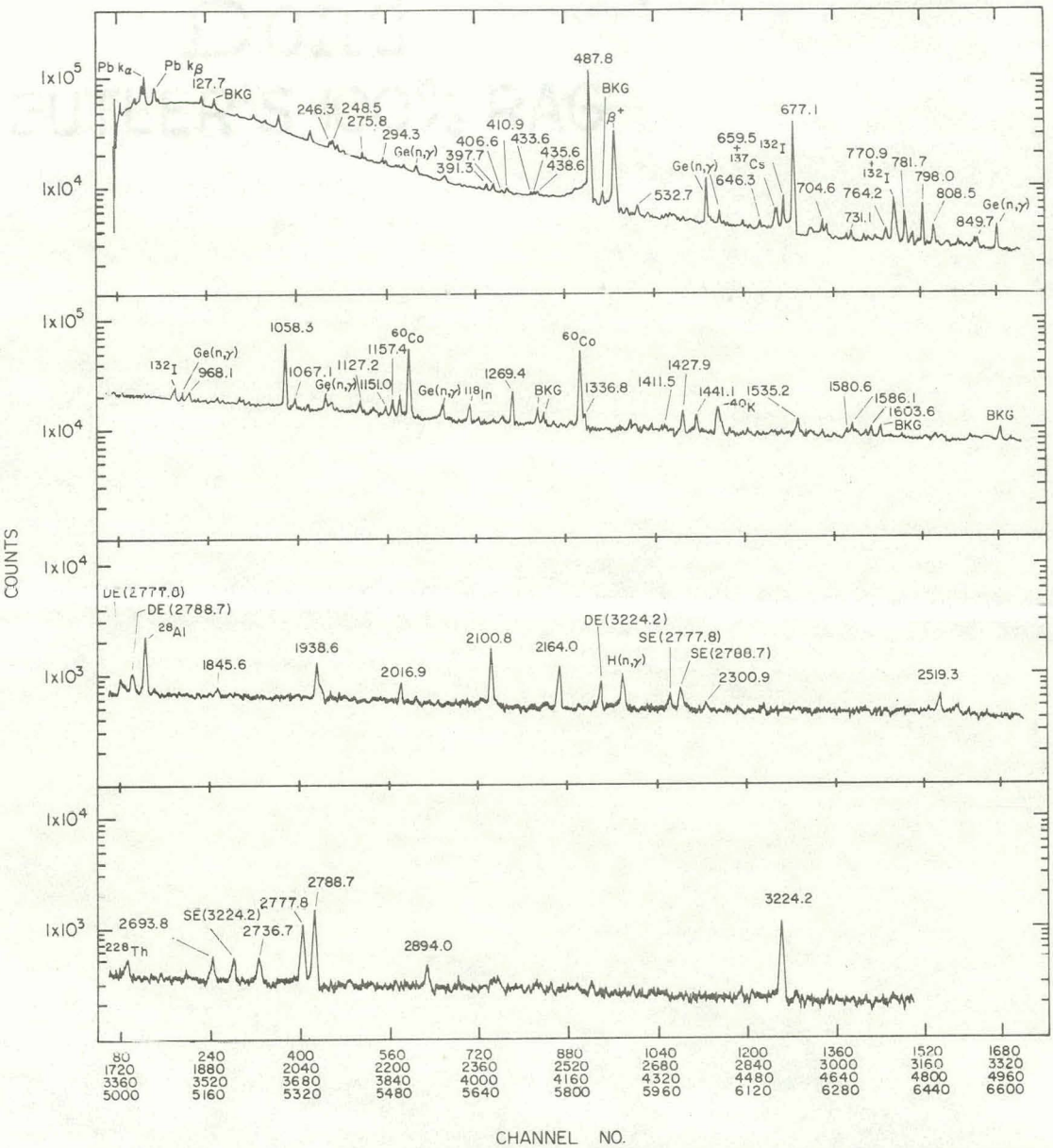

Figure 8. Ge(Li) spectrum from the decay of ^{118}Ag

The computer programs PEAKFIND (12) and SKEWGAUSS (13) were next used to determine peak locations and areas and their errors in the calibration, mixed calibration, and unknown singles spectra. PEAKFIND searches for peaks and performs the initial peak fits. SKEWGAUSS utilizes PEAKFIND output and offers more fitting parameter options for improving peak fits. Both programs generate plots for use in judging the fit quality and card output for use in the program DRUDGE.

DRUDGE converts peak locations and areas into gamma energies and intensities. In order to accurately determine the Ag energies, DRUDGE was submitted to the computer three times. In its first run, DRUDGE determined a relationship between energy and channel number. Intense calibration peaks were used to establish a least-squares (LSQ) line, and other calibration peaks were used to establish the nonlinearity relative to the LSQ line. The local nonlinearities were calculated by hand by subtracting the calibration peaks' LSQ energies from their known energies, and a nonlinearity curve of ΔE versus E(LSQ) was plotted.

Next DRUDGE was run using peaks from the mixed calibration spectrum. This run determined the energies of intense Ag peaks using the calibration peaks as an internal calibration. The LSQ line was established using the same calibration peaks as before, and the positions of several strong Ag

peaks were located on it. At this time, a new nonlinearity curve was also calculated in order to check that the same nonlinearities still applied.

These intense Ag peaks were in turn used to transfer the calibration line to the unknown spectrum in the final DRUDGE run. The nonlinearities were specified by (ΔE,E(LSQ)) pairs chosen from the nonlinearity plot. The program approximated the curve by linear interpolation between these points. This DRUDGE run located the Ag peaks on the calibration line, corrected the LSQ energies for nonlinearities, and generated the final Ag energies.

The final Ag intensities were also calculated during this run. A table of detector efficiencies and uncertainties versus energy was supplied to the program. A table of experimental attenuations due to the 1.6 mm aluminum window in the MTC was also calculated using attenuation coefficients from Siegbahn (14). DRUDGE used this information to convert peak areas into relative intensities. The most intense transition was normalized to 1000. The gamma energies and intensities are summarized in Table I.

Contaminant peaks in the unknown spectrum were identified using various methods. The unknown spectrum was compared with background spectra taken at the parent and daughter ports of the MTC. It was also compared with the daughter spectrum, which was taken using a different MTC enhance-

Table I. Gamma transitions observed in the decay of ^{118}Ag

Energy (keV) this work	Relative[1] intensity	Energy (keV) Ref. (7)	Placement (keV)
246.25 ± 0.09	13.3 ± 1.8		2181-->1936
248.54 ± 0.09	23.2 ± 1.9		unplaced
275.81 ± 0.13	10.7 ± 2.3		3032-->2756
294.30 ± 0.12	12.6 ± 2.0		2223-->1929
391.29 ± 0.11	10.6 ± 1.3		3032-->2640
397.69 ± 0.11	12.7 ± 1.4		2621-->2223
406.6 ± 0.5	2.7 ± 1.8		2322-->1916
410.86 ± 0.18	8.8 ± 2.0		3032-->2621
433.57 ± 0.25	4.6 ± 1.5		2756-->2322
435.59 ± 0.25	5.1 ± 1.5		3224-->2789
438.64 ± 0.16	7.7 ± 1.6		unplaced
487.82 ± 0.06	1000	487.8	488--> 0
532.69 ± 0.15	15.8 ± 3.0		2756-->2223
646.27 ± 0.17	7.8 ± 2.4		1916-->1270
659.54 ± 0.08	27 ± 3		1929-->1270
677.08 ± 0.06	461 ± 25	677.1	1165--> 488
704.55 ± 0.09	16.5 ± 2.0		2640-->1936
731.1 ± 0.3	11.5 ± 3.9		unplaced
764.24 ± 0.15	16 ± 3		1929-->1165
770.95 ± 0.08	74 ± 7	771.1	1936-->1165
781.67 ± 0.08	48 ± 4	781.9	1270--> 488
798.00 ± 0.07	66 ± 5	797.8	1286--> 488
808.52 ± 0.10	26 ± 3	808.3	3032-->2223
849.66 ± 0.13	11.6 ± 2.0		3032-->2182
968.08 ± 0.21	11.7 ± 2.2		unplaced
1058.28 ± 0.09	117 ± 8	1058.4	2223-->1165
1067.1 ± 0.5	14.4 ± 5.0		unplaced
1127.20 ± 0.25	15.6 ± 4.4		unplaced
1151.0 ± 0.3	8.2 ± 2.4		unplaced
1157.43 ± 0.15	17.3 ± 2.5		2322-->1165
1269.38 ± 0.11	33 ± 3	1269.7	1270--> 0
1336.8 ± 0.3	10.5 ± 2.8		3266-->1929
1411.5 ± 0.4	3.3 ± 1.5		unplaced
1427.87 ± 0.20	20 ± 2		1916--> 488
1441.11 ± 0.18	13 ± 1		1929--> 488

[1]Intensities normalized to 1000 for the 488-keV gamma ray.

Table I. (continued)

Energy (keV) this work	Relative[1] intensity	Energy (keV) Ref. (7)	Placement (keV)
1535.2 ± 0.4	19.6 ± 6.5		unplaced
1580.6 ± 0.4	5.4 ± 2.0		unplaced
1586.1 ± 0.4	8.6 ± 2.3		unplaced
1603.6 ± 0.4	8.4 ± 2.3		unplaced
1845.6 ± 0.6	8.8 ± 2.5		unplaced
1938.6 ± 0.3	39 ± 4		3224-->1286
2016.9 ± 0.5	13.6 ± 4.0		3182-->1165
2100.8 ± 0.3	81 ± 6		3266-->1165
2164.0 ± 0.3	40 ± 5		3329-->1165
2300.8 ± 0.4	6.8 ± 2.0		2789--> 488
2519.3 ± 0.3	18.3 ± 4.5		unplaced
2693.8 ± 0.4	25 ± 4		3182--> 488
2736.7 ± 0.3	21 ± 3		3224--> 488
2777.80 ± 0.20	82 ± 7		3266--> 488
2788.70 ± 0.18	125 ± 9		2789--> 0
2894.0 ± 0.3	20 ± 5		3382--> 488
3224.20 ± 0.25	112 ± 9		3224--> 0

ment. Peaks which did not die out with the other Ag peaks belonged to either the daughter or some contaminant. Identifications were also made using the results from other fission-product decay studies.

Some of the intruder peaks were due to reactor or environmental background: ^{28}Al, ^{40}K, ^{60}Co, ^{137}Cs, and ^{228}Th. Peaks resulting from neutron capture in hydrogen and germanium also appeared. Gammas from ^{132}I were also observed. This contamination probably occurred as the beam was being tuned prior to the run.

B. Multiscale Analysis

The MCA multiscale data were recorded on magnetic tape. There were two multiscale records: one for the long-lived decay and one for the short-lived decay. DISKRITE transferred the records from tape to private disk. Plots were obtained of all the energy spectra associated with the 16 time bins. The half-life for the short-lived decay was determined by the decay of the 128-keV peak. The half-life for the long-lived decay was determined from the decay of the 488-keV peak. PEAKFIND and SKEWGAUSS were used to obtain the areas of the 128-, 488-keV, and annihilation peaks in each time-bin spectrum. The annihilation peak (almost entirely from reactor background) areas were checked for any trends that would indicate that systematic errors were affecting the 128-keV and 488-keV decay histories.

For each energy, a line giving the log of the peak area as a function of time was calculated by a simple weighted least-squares program obtained from Bevington (15). From the slope of each LSQ line, the decay half-life was calculated. The decay curves for the 128-keV peak and the 488-keV peak are shown in Figure 9. From the 128-keV line, the half-life of the short-lived decay was calculated to be 2.0 ± 0.2 seconds. This is smaller than the Studsvik value, which was 2.8 ± 0.3 seconds. From the 488-keV line, the

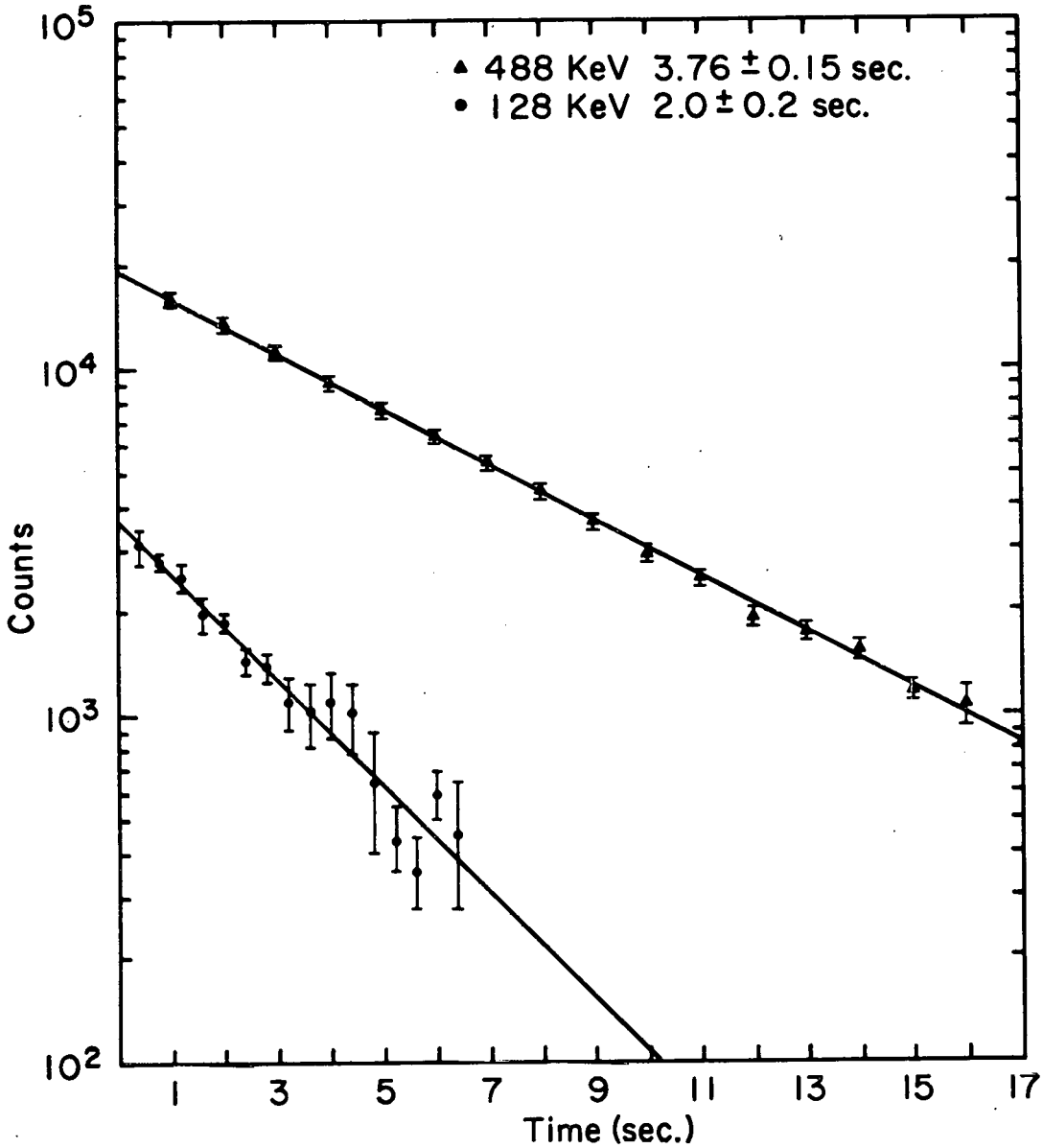

Figure 9. Decay curves for ^{118}Ag

ground state half-life was calculated to be 3.76 ± 0.15 seconds. This value is in good agreement with the Studsvik value of 3.7 ± 0.2 seconds. The half-life for the 488-keV peak was also calculated from the short-lived decay data. This half-life was determined to be 3.8 ± 0.5 seconds, and it agrees well with this study's other value. The half-life for the 128-keV peak was not calculated from the long-lived decay data since the peak's intensity in that data was statistically very poor.

C. Gamma-Gamma Coincidence Data

The two pulse-height spectra from the ADC's, gated by the output of the coincidence circuitry, were recorded on magnetic tape and transferred to private disk by DISKRITE. Since one ADC was labeled "A" and the other "B," the two spectra were called the A and B coincidence profiles. Through UNIPLOT, plots of these coincidence profiles were obtained. One of the plots was used to determine the channel boundaries of the coincidence gates. Two gates were set up for each transition. One was defined by the peak. The other was the same width as the energy gate but was located in an area above the peak to identify coincidences due to the Compton background. These gates were input into the program BUFFTAPE.

Each coincidence event was recorded on a buffer tape as a pair of channel numbers. One channel number was labeled "A" and the other was labeled "B," depending on the origin of the corresponding address. BUFFTAPE read the buffer tape and assembled the appropriate coincidence events for each gate. For example if the A profile was used to index the gates, BUFFTAPE accumulated all the (A,B) pairs in which the A channel number fell inside the boundaries of a particular gate. It added the counts in the B channels and assembled a coincidence spectrum. The program then wrote the coincidence slice on another magnetic tape. The program BUFFREAD was used to read this tape and record the coincidence slices on private disk. All energy and Compton coincidence slices were plotted using UNIPLOT. The coincidence slices for the 488-keV and 2778-keV peaks are shown in Figure 10. The plots were examined to identify coincidences. The coincidence was called definite if the peak was clearly larger in the energy gate slice than in the Compton gate spectrum. If the coincidence peak was only slightly larger or statistically shaky, it was called a possible coincidence. The observed coincidences are listed in Table II.

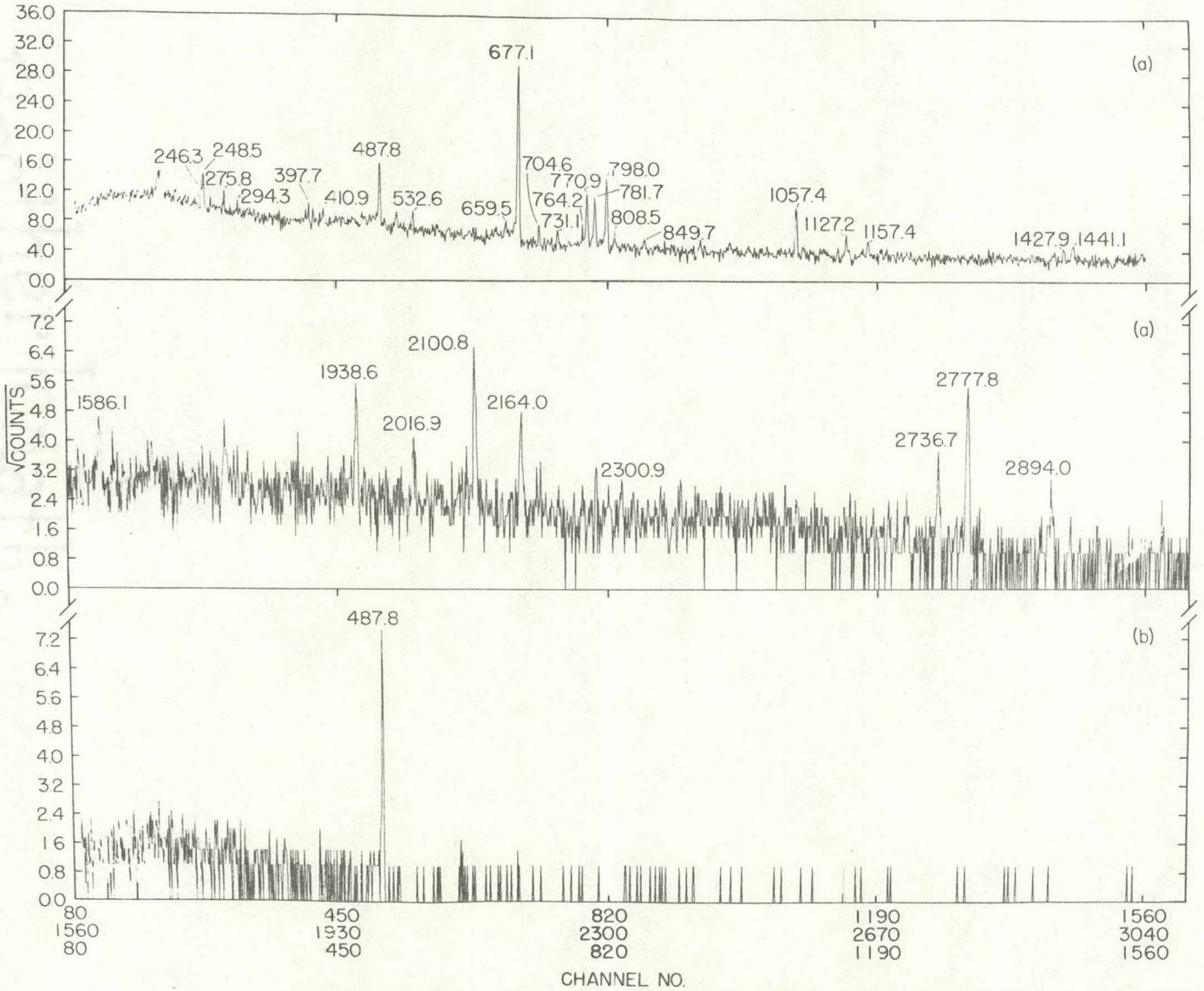

Figure 10. Gamma spectrum in coincidence with the (a) 488-, and (b) 2778-keV gamma rays from the decay of ^{116}Ag

Table II. Coincidences observed in the decay of ^{118}Ag

Gating Energy (keV)	Definite Coincidences (keV)	Possible Coincidences (keV)
246	488,677,771,850	439
249	488,677,1058	
276	407,488,533,660,677, 764,782,1058,1157,1269	434
294	398,660,764,782,809,1269	488
391	677,705,771	488
398	411,488,677,1058	246
407	1428	646,1269
411	398,488,677,1058	
435+436	276,677,1157,2789	488
439	246,1058	677
488	246,249,276,294,398, 411,533,660,677,705, 731,764,771,782,798, 809,850,1058,1127,1157, 1428,1441,1586,1939,2017, 2101,2164,2301,2737,2778, 2894	407,1151,1535, 2694
533	276,488,677,1058	660
646	782,1269	488
660	294,488,782,1269,1337	
677	246,249,276,398,411, 439,488,533,705,731, 764,771,809,850,1058, 1157,2101,2164	
705	391,488,677,771	
731	488,677,1058	
764	488,677	294,1337
771	246,488,677,705,850	391
782	488,646,660	294
798	488,1939	
809	488,677,1058	294
850	246,677,771	249,488
1058	249,398,411,439,488, 533,677,809	731
1127	488	
1157	488,677	434
1269	660,646	

Table II. (continued)

Gating Energy (keV)	Definite Coincidences (keV)	Possible Coincidences (keV)
1337	488,660	764
1428	488	407
1441	488	
1535	488	677
1586		488
1939	488,798	
2017	488,677	
2101	488,677	
2164	488,677	
2301	488	
2694	488	
2737	488	
2778	488	
2789	436	
2894	488	

IV. DECAY SCHEME

A. Level Scheme Construction

Using the results of the singles and coincidence experiments, a level scheme was constructed. The computer program LVLSURCH was used to extend the scheme. The program found new levels by searching for sums of gamma energies which equaled other gamma energies or sums. These combinations were used to establish new levels which were in turn employed in the next iteration. Typical energy matches for cascades of 0.5 keV were required. The number of in- and out-going transitions needed to establish a level were also specified. If a LVLSURCH level agreed with coincidence evidence, it was adopted. The program was particularly useful for locating unplaced gammas in the already established decay scheme.

The decay scheme is shown in Figure 11. In this figure, dots appear at the extremities of the gamma transition arrows. A dot is solid if at least one definite coincidence was observed. A hollow dot indicates that only a possible coincidence was observed.

The spin and parity assignments for this decay scheme were guided by observed gamma transitions and systematics. Knowledge of the percentage of beta feeding to a level also aids the selection of a spin and parity for that level.

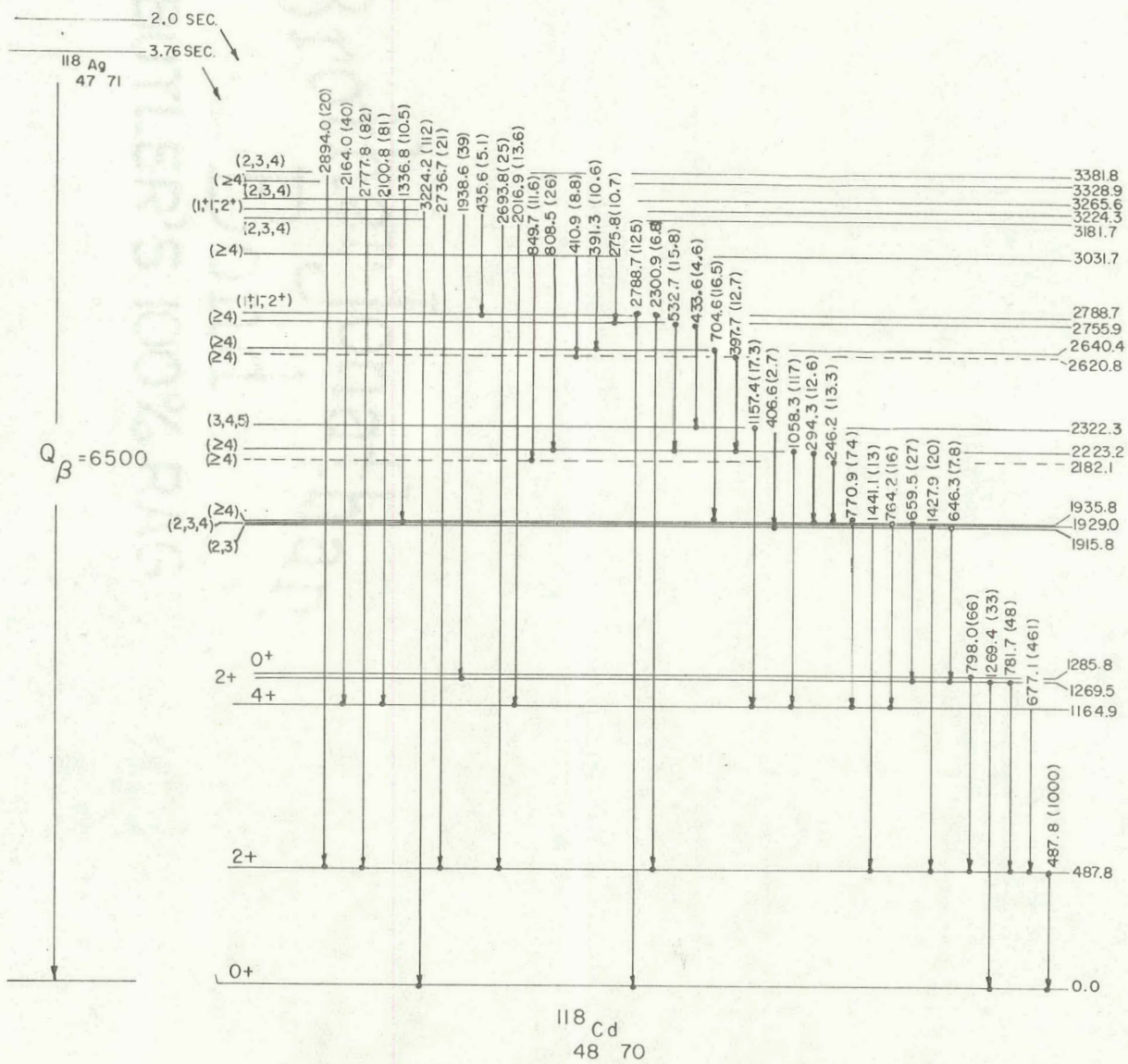

Figure 11. ^{118}Ag decay scheme

This information is necessary for calculating the log*ft* value associated with the level. Log*ft* rules for spin and parity assignments can then be applied to limit choices of possible J^{π}'s.

Beta branchings are difficult to calculate for the decay of ^{118}Ag since there are two isomers involved. The 128-keV isomeric state gamma decays to the Ag ground state. This isomeric transition was observed, and from conversion coefficients and conversion ratios it was found to have multipolarity E3 (7). The spin of the short-lived isomeric state therefore differs from that of the ground state by three units.

Since ^{118}Ag also beta decays from both the isomeric states, gammas from the two decays have to be separated. As described in Chapter II, a one-hour singles experiment was conducted to collect the data needed for this task. The two spectra resulting from the run were plotted, and the parent-port spectrum was compared to the daughter-port spectrum. Since the short-lived decay was suppressed in the daughter-port spectrum, gammas which appeared in both spectra were probably either "mixed" or from the ground state beta decay. An additional complication is due to the fact that the ^{118}Ag ground state grows in due to population by gamma decay from the ^{118}Ag excited-state isomer. By carefully considering the intensity ratios of gamma rays from the

parent and daughter port spectra, we should be able to determine if the level is beta-fed by the long-lived isomer, the short-lived isomer, or both isomers. We will then be able to determine a separate set of log*ft*'s for the beta decay of each isomer. Then the spins and parities can be much more accurately pinned down. The above analysis will be made before submission of this decay scheme for journal publication.

B. The Level Scheme of ^{118}Cd

The spin and parity for the ground state of ^{118}Cd was assumed to be 0^+ since this is the J^π for the ground state of all even-even nuclei.

The most intense gamma ray from the decay of ^{118}Ag at 488 keV was postulated to depopulate the first excited state. This level is almost certainly a 2^+ state since most even-even nuclei have 2^+ first excited states. The main exceptions to this rule are doubly-magic nuclei. Also, all other known even-even Cd nuclei have $J^\pi=2^+$ for the first excited state.

Even-even Cd nuclei display vibrational-type spectra. One expects to see a 0^+-2^+-4^+ triplet at about twice the energy of the first excited state, thus the next three levels at 1165, 1270, and 1286 keV are probably members of this triplet. The J^π of the 1270-keV level is probably 2^+ since

it decays to both the first excited state and the ground state. The 1165- and 1286-keV levels decay to the 2^+ first excited state but do not directly decay to the 0^+ ground state. The 3224-keV level is the only energy level which gamma decays to the 1286-keV level. Its other out-going transitions decay to the 2^+ first excited state and the 0^+ ground state. This level is probably a low spin state which prefers to decay to other low spin states. The J^π of the 1286-keV level is therefore probably 0^+. None of the levels which gamma decay to the 1165-keV level have out-going transitions to the 0^+ ground state. Some of them do decay to the 2^+ first excited state. None of them, however, decay to the 1286- or 1270-keV states which probably have J^π's of 0^+ and 2^+, respectively. These levels are likely to be high spin states which prefer to decay to other high spin states. The J^π of the 1165-keV level is thus probably 4^+.

The 1916-keV level decays to the 2^+ state at 1270 keV and the 2^+ first excited state. It cannot have J=1 since no transition to the ground state is observed. It does not have $J \geq 4$ since there is no transition to the 4^+ 1165-keV level. It is therefore a low spin state with J=2 or 3.

The 1929-, 3182-, 3266-, and 3382-keV levels decay to the 2^+ first excited state and the 4^+ state at 1165 keV. They do not decay directly to the ground state. The most probable spin assignments for these states are J=2, 3, or 4.

The 1936- and 3328-keV levels decay only to the 4^+ state at 1165 keV. They are thus high spin states with $J \geq 4$.

The 2182- and 2640-keV levels decay only to the high spin state at 1936-keV. They are also likely to be high spin states with $J \geq 4$.

The 2223-keV level decays to the 4^+ state at 1165 keV and the high spin state at 1929 keV. It is probably a high spin state with $J \geq 4$.

The 2322-keV level decays to the 4^+ state at 1165 keV and the J=2 or 3 state at 1916 keV. It probably has J=3, 4, or 5.

The 2621- and 2756-keV levels both decay to the high spin state at 2223 keV. They probably have $J \geq 4$.

The 2789- and 3224-keV levels decay to both the ground state and the first excited state. Possible spin and parity assignments are 1^+, 1^-, and 2^+. The spin and parities 0^+ and 0^- are not possible choices since a $0^\pm$ to 0^+ transition is forbidden. (A phonon has spin 1 and thus must be able to carry off at least one unit of spin.) A J^π of 2^- is also a poor choice since a 2^- to ground state (0^+) transition has multipolarity M2 and a 2^- to first excited state (2^+) transition has multipolarity E1. An M2 transition generally does not compete with an E1 transition, thus transitions from these levels to the ground state would not be observed if they had $J^\pi = 2^-$.

The 3032-keV level decays to four high spin states at 2182-,2621-, 2640-, and 2756-keV. It is also likely to be a high spin state with J≥4.

The coincidence evidence for the two levels at 2621 keV and 2182 keV is not totally convincing even though the energy matches are quite good. The 411- and 398-keV gammas, which are in coincidence, cascade from the 3032-keV level, implying a level at either 2621 or 2634 keV. The level at 2621 keV was eventually chosen because of a more favorable intensity balance. Additional evidence for such an ordering was the placement of the 439-keV gamma ray between the 2621- and 2182-keV levels, but the coincidence information for the 439-keV gate was not consistent with this placement and the 439-keV gamma ray was not included in the level scheme. The 850- and 246-keV gamma rays, which are in coincidence, also cascade from the 3032-keV level, implying a level at either 2182 or 2785 keV. Again the above placement of the 439-keV gamma ray would favor the 2182-keV level, but the final decision was based on the intensity balance. The two levels at 2621 keV and 2182 keV are thus not well-established and are dashed in the level scheme figure.

V. DISCUSSION

A. Comparison with Previous Work

The levels proposed in the study are compared to the beta-decay results of Fogelberg, et al. (7) in Figure 12. Thirty-one new gamma-ray transitions and fourteen new levels were found. The previous study's level at 1973 keV was not supported by new experimental results. In particular, the new coincidence information did not support the 808-keV transition from the 1973-keV level. The remaining levels, their spins and parities, and their gamma transitions are in fairly good agreement with the present study's findings. The gamma intensities cannot be compared, since they were not given in the previous work.

B. ^{118}Cd and the Davydov-Chaban Model

Medium-weight ($50<A<150$) even-even nuclei near closed shells are typically classified as vibrational nuclei. They are characterized as vibrational because of several properties they share: (1) They generally possess low-lying first-excited states with spin and parity 2^+. (2) There is a triplet of excited states at approximately twice the energy of the first excited state with spins and parities of 0^+, 2^+, and 4^+. The levels are characteristic of a quadrupole vibrator. The energy states of the vibrator are

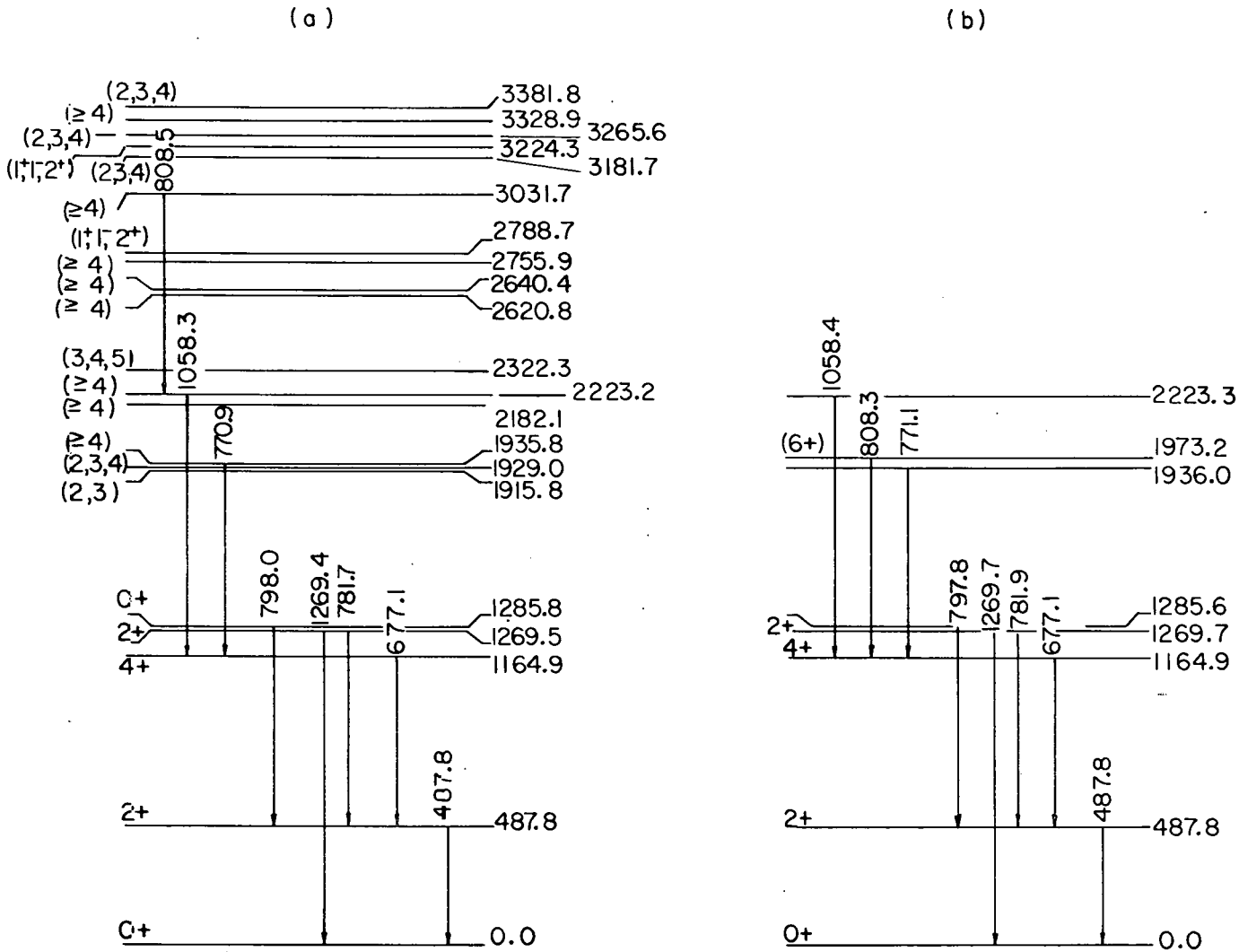

Figure 12. Comparison of ^{118}Cd levels with those from previous work (a) this work, (b) Ref. (7)

identified by phonon numbers, which indicate the number of quanta of vibrational excitation. In an ideal vibrational nucleus, the two- and three-phonon states are degenerate multiplets, however real vibrational nuclei have nondegenerate phonon multiplets. The 0^+-2^+-4^+ triplet corresponds to the two-phonon multiplet. Also, the energy ratio of the center of gravity of the two-phonon multiplet to the first excited state is generally a little greater than two.

Some even-even nuclei are rotational in character. For a pure rotational nucleus, the energy ratio of two excited states is given by the equation:

$$\frac{E(J_2)}{E(J_1)} = \frac{J_2(J_2+1)}{J_1(J_1+1)}$$

Thus for a pure rotator $E(4^+)/E(2^+)=3.33$, whereas for a pure vibrator $E(4^+)/E(2^+)=2.0$. From this study's experimental results for ^{118}Cd, the energy ratio $E(4^+)/E(2^+)=2.39$. Furthermore, a nondegenerate 4^+-2^+-0^+ triplet suggestive of the two-phonon multiplet is present. Thus ^{118}Cd clearly tends to be vibrational in character. This is to be expected since Cd (Z=48) is only two proton numbers away from the magic number Z=50, thus its nucleus is almost spherical. Rotational behavior is not seen in spherical nuclei, so rotational effects should be small in Cd.

Collective rotations are reasonably well-described by a quantum mechanical rotor. The starting point of any vibra-

tional description of collective motion is usually Bohr's harmonic quadrupole-surface oscillator model, however a wide variety of anharmonic terms have been added by various authors. No single model with anharmonic terms appears to apply to all nuclei. The theoretical approach considered in this study is the Davydov-Chaban model (1,2). In the Davydov-Chaban model, the nuclear surface is assumed to possess a quadrupole equilibrium shape. Five real coordinates are required to specify the appearance of a general quadrupole surface relative to a set of laboratory axes. These may be taken to be the Bohr coordinates (β,γ,Θ_i). The Euler angles $(\Theta_1,\Theta_2,\Theta_3)$ specify the orientation of a set of body-fixed (BF) principal axes while the shape parameters β and γ dictate the appearance of the surface to a BF observer. β is a measure of the overall deformation from sphericity ($\beta=0$) and γ indicates the degree of rotational asymmetry about the BF z-axis. Quadrupole surfaces, as they appear in the BF frame, are depicted in Ref. 16 for various values of the pair (β,γ). Within the framework of the Davydov-Chaban model, β and the Θ_i are treated as dynamical variables. The asymmetry parameter γ, however, is viewed as a constant. The model consequently couples breathing mode vibrations (β-vibrations) with asymmetric rotor motion. The energy spectrum is dependent upon three model parameters: the asymmetry γ, an overall energy scale factor $\hbar\omega$, and the

nonadiabaticity parameter μ. The latter is a measure of the stiffness of the β-vibrator to centripetal stretching. When $\mu=0$, no such stretching occurs. In this limit the β-vibrations and rotations are completely uncoupled. The potential energy in β depends upon a centrifugal barrier whose height is dictated by the rotational energy together with a parabolic potential in β involving an equilibrium value β_0. The parameter μ arises when we approximate this total potential by a single parabolic potential with an equilibrium value β_0' which depends upon the rotational energy. If $\mu \leq 0.5$ this approximation is quite good. For larger values of μ, the resultant mathematical model is completely tractable but is only a rough approximation to the original Hamiltonian. The angular parameter γ may be restricted to $0^\circ \leq \gamma \leq 30^\circ$ by symmetry properties of the nuclear surface and the corresponding Hamiltonian. At the lower limit, the quadrupole surface has rotational symmetry about the BF z-axis for all values of β.

A typical energy spectrum of the Davydov-Chaban model may be partitioned into rotational bands each of which is based upon a $J=0$ β-vibrational state. Every such band consists of $(J+2)/2$ states of each even spin and $(J-1)/2$ states of each odd spin. In the limit $\mu=0$, the purely vibrational states (the β-bandheads) are equally spaced in energy, and each rotational band is that of a quadrupole rotor. The experimental energies designated by "*" in Figure 13 have been

used in the determination of the three model parameters μ, γ, and $\hbar\omega$. These were found to be 0.99, 20.9°, and 866 keV respectively. Because μ=0.99 the approximate Hamiltonian and the original Hamiltonian differ somewhat. The effect of this difference could be assessed by first order perturbation corrections to the energy levels, but this has not been done. The equilibrium value of β, a measure of the nuclear deformation, cannot be determined without an accompanying measurement of an absolute E2 transition rate or the intrinsic quadrupole moment.

A comparison for ^{118}Cd between results from this experiment and those obtained by S. A. Williams from the model is shown in Figure 13. Since the nuclear quadrupole surface has inversion symmetry about the z-axis, the parities of the theoretical spin assignments are positive. Note that the experimental 488-, 1165-, 1270-, 1286-, 1916-, 1929-, and 1936-keV levels were used in the fitting procedure. These states were assumed to have J=2, 4, 2, 0, 4, 2, and 6, respectively.

The model predicts three states at 1174, 1268, and 1405 keV which have J=4, 2, and 0, respectively. These levels correspond to the 4$^+$ 1165-, 2$^+$ 1270-, and 0$^+$ 1286-keV experimental states. The agreement between energies and spins is quite good with the exception of the 1405-keV level, which

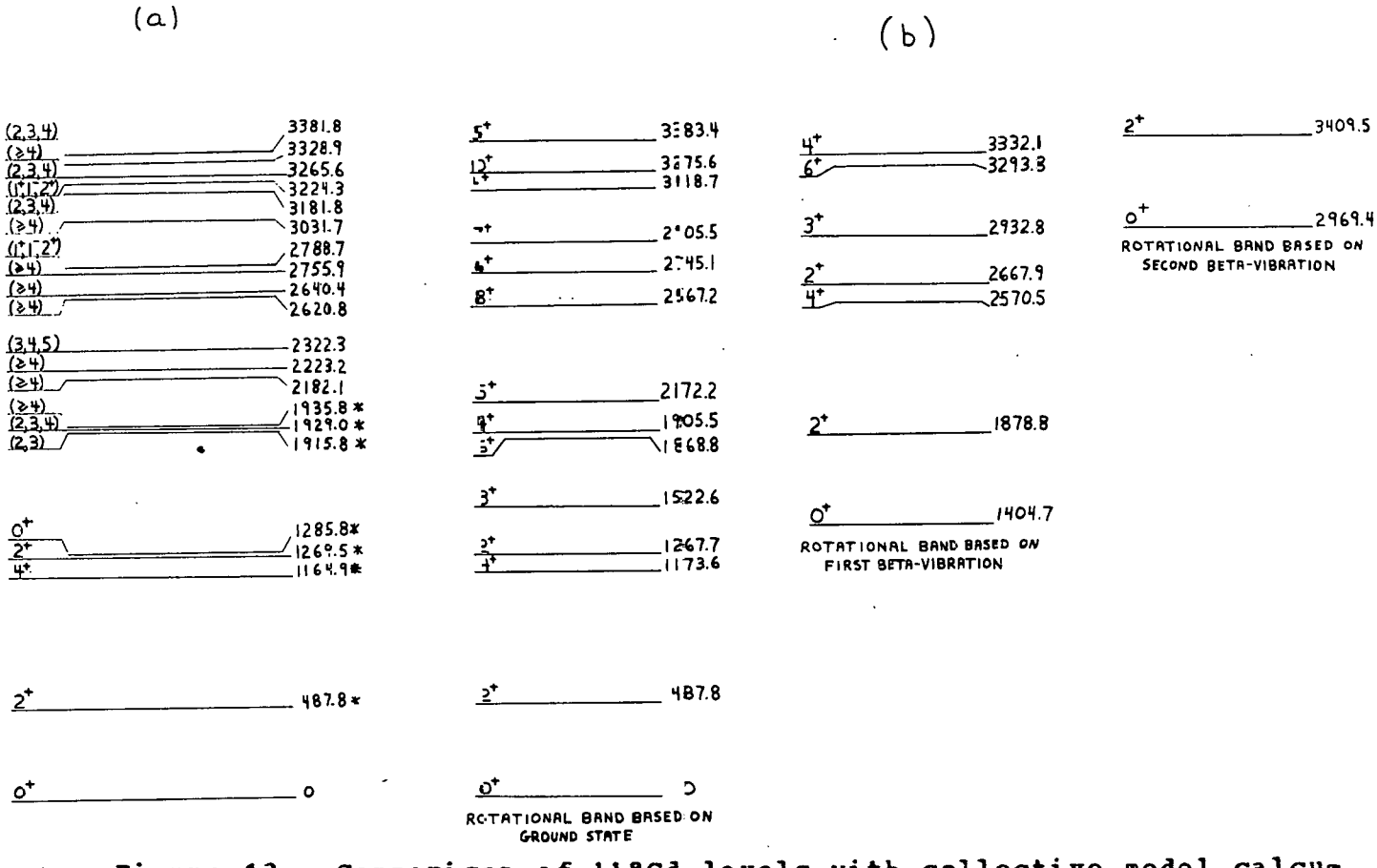

Figure 13. Comparison of ^{118}Cd levels with collective model calculations (a) experiment, (b) theory

is a little too high in energy.

The theoretical J=3 state at 1523 keV was not observed. It is possible that this level was not populated in this particular experiment and may yet be detected in some other type of decay study.

The model predicts three states at 1869, 1879, and 1906 keV which have J=6, 2, and 4, respectively. There are three experimental levels at about these energies, the levels at 1916, 1929, and 1936 keV. The experimental spin assignments agree quantitatively with the theoretical spins, but they are ordered differently.

The model calculates a J=5 state at 2172 keV. Three high-spin experimental levels, however, were observed in the vicinity of this energy. The 2182-, 2232-, and 2322-keV levels were all assigned J≥4. The model clearly computes too small a level density for this energy region. This indicates that another degree of freedom is needed for fitting this nucleus. There is probably some single particle motion in addition to the collective motion of the nucleus. Two of these levels probably depend strongly on single-particle motion effects, thus the model does not calculate them.

The model next predicts three high-spin states and one low-spin state. These occur at 2567, 2570, 2668, and 2745 keV and have J=8, 4, 2, and 6, respectively. The experimental level scheme has three high-spin states and one low-spin

state at slightly higher energies. The high-spin states are at 2621, 2640, and 2756 keV. The low-spin state is at 2789 keV. Except for the ordering of the low spin state, the model's calculations are qualitatively quite good.

The model calculates three low-spin states and six high-spin states between 2900 and 3500 keV. The low-spin states are at 2932, 2969, and 3410 keV and they have J=3, 0, and 2, respectively. Only one experimental low-spin state was definitely observed. This level was at 3224 keV and had $J^{\pi}=1^{+}$, 1^{-}, or 2^{+}. It may correspond to the theoretical level at 3410 keV. Three experimental levels at 3182, 3266, and 3382 with J=2, 3, or 4 were observed. They are potentially either low-spin or high-spin states, however no J=0 state was observed. The six high-spin theoretical states are at 2906, 3119, 3276, 3294, 3332, and 3383 keV and they have J=7, 4, 10, 6, 4, and 5, respectively. Only two experimental levels at 3032 and 3329 keV definitely have $J \geq 4$. It is difficult to judge the model's success in fitting these energy levels since the experimental spin assignments are rather vague. The model clearly predicts too many levels, however some of these, particularly the J=0 state, may not have been populated in this experiment.

In general, the model provides a fair description of the energy states of the ^{118}Cd nucleus. Even though its calculations do not fit the experimental results exactly,

the model does present a good picture of the qualitative features of the level scheme.

C. Systematics

Figure 14 compares the ^{118}Cd level scheme developed in this study with the level schemes of other even-even Cd nuclides. Note that the energy of the first excited state has a minimum at ^{118}Cd(N=70). ^{120}Cd(N=72) has a first excited state that is close in energy to the first excited state of ^{116}Cd(N=68). The first excited states of ^{114}Cd(N=66) and ^{122}Cd(N=74) are also close in energy. It appears that adding a pair of neutrons to the ^{118}Cd nucleus has the same effect on the first excited state as removing a pair of neutrons.

The 4^+ state follows an energy trend similar to that of the first excited state. It also has a minimum in energy at ^{118}Cd. The fact that the energy of the 4^+ state rises and falls with that of the 2^+ first excited state indicates that these levels have strong collective character. If they were particle states, they would not exhibit this behavior. One might expect the energy minimum of these states to occur at ^{114}Cd, which is midway between the N=50 and N=82 closed shells, but they are instead slightly displaced to the

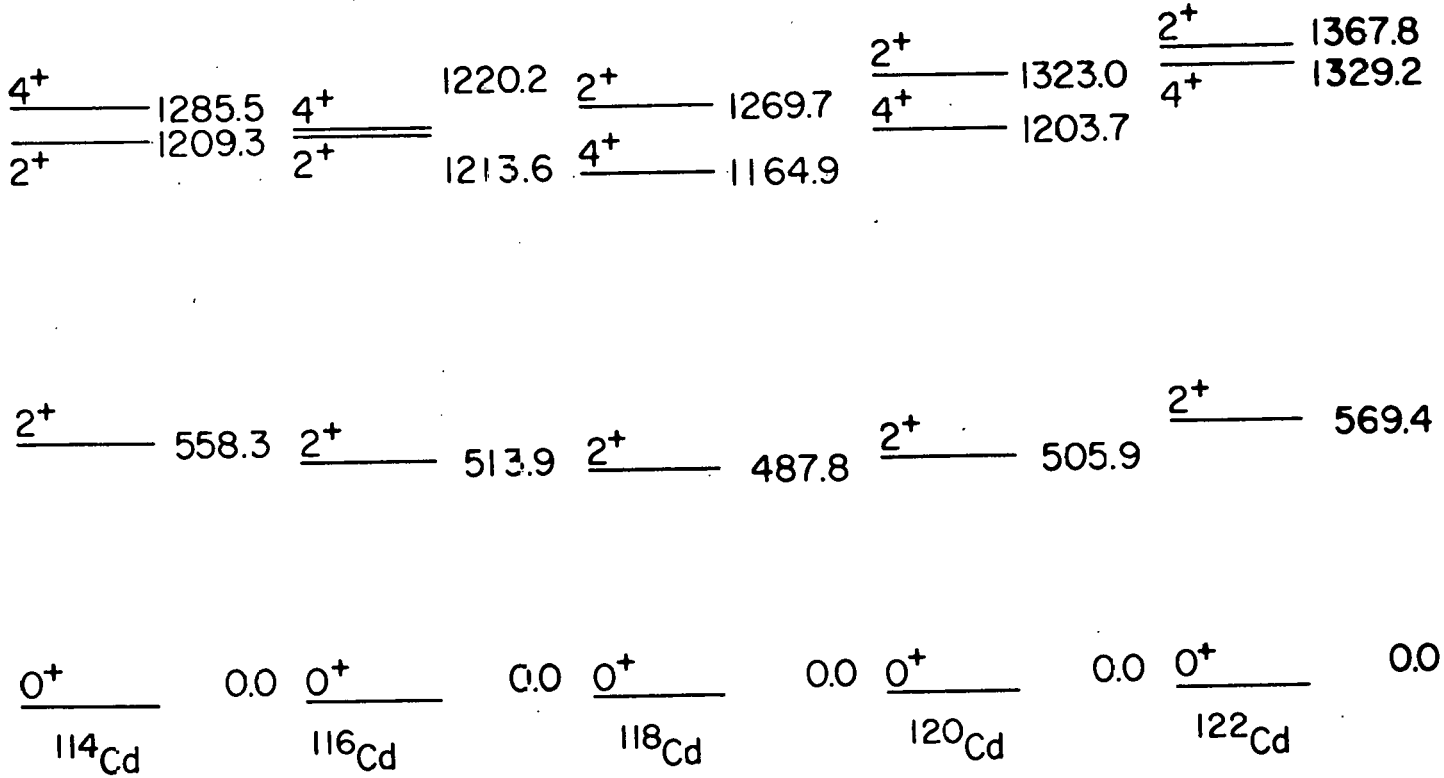

Figure 14. Systematics of even-even Cd isotopes

neutron-rich side. We can understand this behavior if we view these levels as rotor states. In this case, the minimum of the first excited state energy at A=118 indicates that this nucleus has a larger effective moment of inertia than the other Cd nuclei. More nucleons outside the core are apparently participating in collective rotations. This energy trend also implies that holes are not the same as particles in so far as participation in collective rotations is concerned.

The second 2^+ state exhibits what one might think of as "normal" behavior. That is, it has an energy minimum at A=114, the middle of the neutron shell. If these Cd nuclei were purely vibrational in character, one would expect this 2^+ state to follow the same trend as the lower 2^+ and 4^+ levels. Since it does not, this is an indication of the rotational character of these states. The energy minimum of the second 2^+ state at A=114 indicates that there is a maximal sort of asymmetry in the momental ellipsoid. That is, the moments of inertia along axes perpendicular to the BF z-axis ($I_\perp$) are larger than the moment of inertia along this axis (I_z). Furthermore as A increases from 114 to 118, the ratio of I_z to $I_\perp$ decreases. The angular momentum of the second 2^+ state has its largest component along the BF z-axis, while the angular momentum of the first 2^+ state has its largest component perpendicular to it. The first 2^+

energy and the second 2^+ energy are then determined primarily by the magnitudes of $I_\perp$ and I_z, respectively. The energy of the first 2^+ state thus falls as A increases from 114 to 118 while the energy of the second 2^+ state rises. In order to understand the behavior of the moments of inertia, we must eventually turn to the shell model and consider the relationship between collective motion and particle-hole excitations.

It would be interesting to see if the trends continue as more neutron pairs are added and the magic neutron number 82 is approached. The TRISTAN group is planning to search for ^{124}Ag with the goal of further investigating the systematics of even-even Cd isotopes.

VI. LITERATURE CITED

1. A. S. Davydov and A. A. Chaban, "Rotation-vibration interaction in non-axial even nuclei," Nucl. Phys. 20, 499 (1960).

2. S. A. Williams and J. P. Davidson, "A generalized rotation-vibration model for deformed even nuclei," Can. J. Phys. 40, 1423 (1962).

3. H. H. Hsu, S. A. Williams, F. K. Wohn, and F. J. Margetan, "The collective structure of the even-mass Pd isotopes," Phys. Rev. 16C, 1626 (1977).

4. K. Fritze and K. Griffiths, "Short-lived fission products," Radiochim. Acta 7, 59 (1967).

5. H. V. Weiss, J. M. Fresco, and W. L. Reichert, "Identification of 5.3-sec ^{118}Ag as a product of ^{235}U fission," Phys. Rev. 172, 1266 (1968).

6. H. V. Weiss, N. E. Ballou, J. L. Elzie, and J. M. Fresco, "Nuclear charge distribution in symmetric fission of ^{235}U with thermal neutrons: yields of ^{117}Ag, ^{118}Ag, and ^{118}Pd," Phys. Rev. 188, 1893 (1969).

7. B. Fogelberg, A. Bäcklin and T. Nagarajan, "Energy levels in $^{114\ 116\ 118\ 120\ 122}$Cd as observed in the beta decay of Ag isotopes," Phys. Letters 36B, 334 (1971).

8. G. Rudstam, "The on-line mass separator OSIRIS and the study of short-lived fission products," Nucl. Instr. Meth., 139, 239 (1976).

9. J. R. McConnell and W. L. Talbert, Jr.," The TRISTAN on-line isotope separator facility," Nucl. Instr. Meth., 128, 227 (1975).

10. D. A. Gedcke and W. J. McDonald, "Constant fraction of pulse height trigger for optimum time resolution," Nucl. Instr. Meth., 55, 377 (1967).

11. D. A. Gedcke and W. J. McDonald, "Design of the constant fraction of pulse height trigger for optimum time resolution," Nucl. Instr. Meth., 58, 253 (1968).

12. W. C. Schick, Jr., "PEAKFIND: A Fortran program for locating and fitting peaks in semiconductor detector

spectra," IS-3636 (1975).

13. W. C. Schick, Jr., "SKEWGAUS: A Fortran program for fitting peaks in semiconductor detector spectra," IS-3460 (1974).

14. K. Siegbahn (ed.), "Alpha-, Beta-, and Gamma-Ray Spectroscopy, Vol. I," (North-Holland Publishing Company, Amsterdam, 1965).

15. P. R. Bevington, "Data reduction and error analysis for the physical sciences," (McGraw-Hill, New York, 1969).

16. T. M. Corrigan, F. J. Margetan, and S. A. Williams, "Exact solution of the quadrupole surface vibration Hamiltonian in body-fixed coordinates," Phys. Rev. 14C, 2279 (1976).

VII. ACKNOWLEDGEMENTS

The author wishes to express her appreciation and thanks to the following people for their contributions to this project:

Dr. John C. Hill for his supervision of this study and his guidance during the writing of this thesis.

M. A. Cullison, Dr. R. L. Gill, A. R. Landin, and D. R. Lekwa for their maintenance of TRISTAN and their assistance in obtaining this data.

M. L. Gartner, Dr. T. K. Li, and L. L. Shih for their assistance during the long hours of data collection.

Dr. S. A. Williams for providing the calculations from the Davydov-Chaban model and his constructive comments on the theory section of this thesis.

Frank J. Margetan for his guidance during the writing of the theory section of this thesis.

Dr. W. L. Talbert, Jr. for his guidance during the early phases of the author's work.

Finally, the author wishes to thank her parents, William and Arlene Reed, for their encouragement and support during her education at Iowa State University.